

## Article

# Development and Validation of a Near-Infrared Spectroscopy Method for Multicomponent Quantification during the Second Alcohol Precipitation Process of *Astragali radix*

Wenlong Li <sup>1,2,3</sup>, Yu Luo <sup>1</sup>, Xi Wang <sup>2</sup>, Xingchu Gong <sup>1</sup> , Wenhua Huang <sup>4</sup>, Guoxiang Wang <sup>4</sup> and Haibin Qu <sup>1,\*</sup>

<sup>1</sup> Pharmaceutical Informatics Institute, College of Pharmaceutical Sciences, Zhejiang University, Hangzhou 310058, China

<sup>2</sup> College of Pharmaceutical Engineering of Traditional Chinese Medicine, Tianjin University of Traditional Chinese Medicine, Tianjin 300193, China

<sup>3</sup> Haihe Laboratory of Modern Chinese Medicine, Tianjin 301617, China

<sup>4</sup> Livzon (Group) Limin Pharmaceutical Factory, Shaoguan 512028, China

\* Correspondence: quhb@zju.edu.cn; Tel./Fax: +86-571-88208428

**Abstract:** The objective of this study was to develop and validate a near-infrared (NIR) spectroscopy based method for in-line quantification during the second alcohol precipitation process of *Astragali radix*. In total, 22 calibration experiments were carefully arranged using a Box–Behnken design. Variations in the raw materials, critical process parameters, and environmental temperature were all included in the experimental design. Two independent validation sets were built for method evaluation. Validation set 1 was used for optimization. Different spectral pretreatments were compared using a “trial-and-error” approach. To reduce the calculation times, the full-factorial design was applied to determine the potential optimal combinations. Then, the best parameters for the pretreatment algorithms were compared and selected. Partial least squares (PLS) regression models were obtained with low complexity and good predictive performance. Validation set 2 was used for a thorough validation of the NIR spectroscopy method. Based on the same validation set, traditional chemometric validation and validation using accuracy profiles were conducted and compared. Conventional chemometric parameters were used to obtain the overall predictive capability of the established models; however, these parameters were insufficient for pharmaceutical regulatory requirements. Then, the method was fully validated according to the ICH Q2(R1) guideline and using the accuracy profile approach, which enabled visual and reliable representation of the future performances of the analytical method. The developed method was able to determine content ranges of 8.44–39.8% at 0.541–2.26 mg/mL, 0.118–0.502 mg/mL, 0.220–0.940 mg/mL, 0.106–0.167 mg/mL, 0.484–0.879 mg/mL, and 0.137–0.320 mg/mL for total solid, calycosin glucoside, formononetin glucoside, 9, 10-dimethoxypterocarpan glucopyranoside, 2'-dihydroxy-3', 4'-dimethoxyisoflavan glucopyranoside, astragloside II, and astragloside IV, respectively. These ranges were specific to the early and middle stages of the second alcohol precipitation process. The method was confirmed to be capable of achieving an in-line prediction with a very acceptable accuracy. The present study demonstrates that accuracy profiles offer a potential approach for the standardization of NIR spectroscopy method validation for traditional Chinese medicines (TCMs).

**Keywords:** near-infrared spectroscopy; *Astragali radix*; alcohol precipitation; validation; accuracy profile



**Citation:** Li, W.; Luo, Y.; Wang, X.; Gong, X.; Huang, W.; Wang, G.; Qu, H. Development and Validation of a Near-Infrared Spectroscopy Method for Multicomponent Quantification during the Second Alcohol Precipitation Process of *Astragali radix*. *Separations* **2022**, *9*, 310. <https://doi.org/10.3390/separations9100310>

Academic Editor: Nguyen Van Quan

Received: 15 August 2022

Accepted: 7 October 2022

Published: 14 October 2022

**Publisher's Note:** MDPI stays neutral with regard to jurisdictional claims in published maps and institutional affiliations.



**Copyright:** © 2022 by the authors. Licensee MDPI, Basel, Switzerland. This article is an open access article distributed under the terms and conditions of the Creative Commons Attribution (CC BY) license (<https://creativecommons.org/licenses/by/4.0/>).

## 1. Introduction

*Astragali radix* is one of the most extensively used Chinese herbal medicines because of its effect of increasing the overall vitality of the system, and it has been prescribed for general debility and chronic illnesses for centuries [1]. In recent years, it has been used clinically for spinal cord injury [2], tissue fibrosis, and other diseases [3]. Alcohol precipitation is a vital separation unit that is widely used in the manufacture of botanical medicines to

purify the water extracts of medicinal plants [4]. In the manufacturing of Chinese patented drugs derived from *Astragali radix*, a second ethanol precipitation is performed after the first ethanol precipitation to remove more impurities, such as saccharides or proteins. The quality of the intermediates in the following processes and the finished products is thought to be affected by the second ethanol precipitation. To ensure a precise and reproducible alcohol precipitation process, the composition of the alcohol precipitation liquid should be closely supervised during the process.

Due to the complicated ingredients in *Astragali radix*, it is insufficient to realize quality control using a single indicator. The total solid (TS) content represents the total soluble solids (mostly saccharides) that are partially removed during the precipitation process. Flavonoids and saponins are bioactive components that are responsible for pharmacological activities and therapeutic efficacy [5,6]. In this study, the contents of TS, four flavonoid compounds, and two saponin compounds were taken as critical quality attributes (CQAs) of the alcohol precipitation liquids. However, these seven quality indices are often determined by the time-consuming, loss-on-drying method or by high-performance liquid chromatography (HPLC), which fail to satisfy the need for real-time monitoring.

With its advantages of nondestructive and high-speed acquisition, near-infrared (NIR) spectroscopy is a good process analytical technology (PAT) tool that has long been used in the pharmaceutical industry. To develop a sound NIR spectroscopy method, representative samples should be carefully selected, which need to be robust with the expected variation [7]. In the modeling, spectral pretreatments should also be properly selected. Among the different types of selection approaches, the “trial-and-error” approach [8] is a fit-for-use oriented approach, which applies all the possible pretreatments to the data set and selects the optimal one according to the goal of the analysis. However, this approach may be computationally intensive.

Prior to routine analysis, the established NIR spectroscopy method should be validated to demonstrate that it is suitable for its intended purpose [9]. However, validation of the chemometric method is not straightforward compared with the validation of conventional analytical techniques, such as chromatography or titrimetry. In pharmaceutical applications, validation based on traditional chemometric parameters is widely used to assess the performance of the developed NIR spectroscopy method [10]. Such parameters include the correlation coefficient (R), root mean square error of calibration (RMSEC), root mean square error of cross-validation (RMSECV), and root mean square error of prediction (RMSEP). However, the model performance evaluation is an area that has not been fully explored. Some studies have demonstrated that all these parameters provide insufficient information to guarantee the suitability of the method for the intended purpose [11–13]. For example, R is an index affected by unwanted factors, such as data distribution. The more centralized the data distribution is, the more difficult it is to obtain a higher R, while the more dispersed the data distribution is, the more likely it is to obtain a higher R.

The validation strategy of an accuracy profile, which was introduced by the commission of the Société Française des Sciences et Techniques Pharmaceutiques (SFSTP) [14–16], involves acquiring the content ranges over which future measurements will be sufficiently accurate. The accuracy profile is based on  $\beta$ -expectation tolerance intervals, which reflect the total measurement error.

A method is considered to be valid when the  $\beta$ -expectation tolerance intervals are fully included within the predefined acceptance limits. As described by De Bleye et al., accuracy profiles have been used for many NIR spectroscopic methods in pharmaceutical applications [10].

In the manufacturing of traditional Chinese medicine (TCM) preparations, NIR spectroscopy has been extensively applied [17]. However, most NIR spectroscopy methods have been considered valid when satisfactory traditional chemometric parameters were obtained, and few of the methods were further validated according to the ICH Q2(R1) guideline. In reported studies, there have been some cases of using the accuracy profile approach during the validation stage, such as methods for the determination of baicalin

in Yinhuang oral solution [18], chlorogenic acid in the ethanol precipitation solution of *Lonicera japonica* [19], and licorice acid in a blending process [20]. However, to our knowledge, there have been few studies that have focused on a thorough validation of an in-line NIR spectroscopy method for multicomponent quantification.

The objective of this study was first to develop an NIR spectroscopy method for multicomponent quantification during the second alcohol precipitation process of *Astragali radix*, meanwhile during which a selection method based on the design of experiments (DOE) was used to reduce the calculation times for the selection of pretreatments. The second aim was to fully validate the in-line method for the seven analytes and to compare the traditional chemometric validation with the accurate profile approach.

## 2. Materials and Methods

### 2.1. Materials

The concentrated supernatants of the first ethanol precipitation of *Astragali radix* were supplied by Livzon (Group), Limin Pharmaceutical Factory (Shaoguan, China). Anhydrous alcohol was purchased from Changqin Chemical Co., Ltd. (Hangzhou, China). Standard substances of calycosin-7-O- $\beta$ -D-glucoside (CG), formononetin-7-O- $\beta$ -D-glucoside (FG), 9,10-dimethoxypterocarpan-3-O- $\beta$ -D-glucopyranoside (DPGP), 2'-dihydroxy-3',4'-dimethoxyisoflavan-7-O- $\beta$ -D-glucopyranoside (DDIFGP), astragaloside II (AG II), and astragaloside IV (AG IV) were purchased from Shanghai Winherb Medical Technology Co., Ltd. (Shanghai, China).

### 2.2. Alcohol Precipitation Process and Experimental Setup

Typical operating conditions for the second alcohol precipitation process were as follows. First, 300 g of concentrated supernatant of the first ethanol precipitation of *Astragali radix* (TS content was 40%) was placed into a 2 L jacketed glass container. The solution was maintained at a constant temperature of 25 °C using a circulation bath. A 95% (v/v) alcohol solution that was 900 g was added into the glass container at a constant speed using a peristaltic pump, and the mixed solution was stirred using a mechanical stirrer at a speed of approximately 350 rpm. The alcohol adding time was 20 min, and the mixed solution was allowed to stand for 10 min without stirring. The supernatant was obtained as the second alcohol precipitation liquid.

The experimental setup is shown schematically in Figure 1. An NIR immersion transreflectance probe with a 2 mm optical path length (Hellma, Müllheim, Germany) was directly inserted into the glass container and connected to the spectrometer by optic fibers. During the precipitation process, a sample of approximately 5 mL was collected near the probe every 5 to 10 min for reference assays.

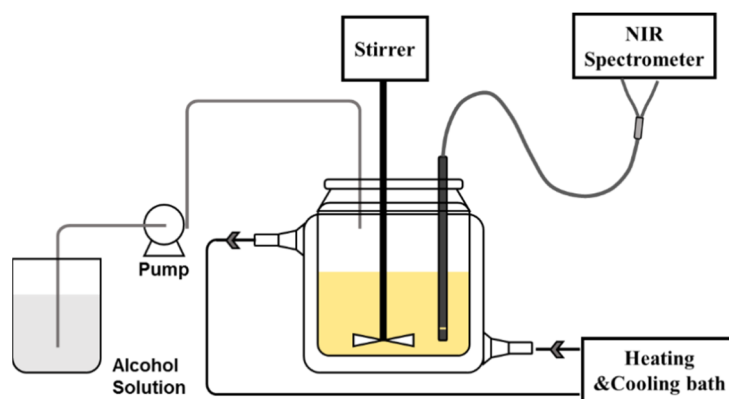


Figure 1. Schematic of the experimental setup for the second alcohol precipitation process.

### 2.3. NIR Spectral Acquisition

NIR spectra were collected in transreflectance mode using an Antaris FT-NIR spectrophotometer (Thermo Nicolet Corporation, Waltham, MA, USA) fitted with an InGaAs detector and a 2 mm optical path length immersion probe. The instrument resolution was specified at  $8\text{ cm}^{-1}$ . Each spectrum was acquired by averaging 32 scans over the wavenumber range of  $4500\text{--}10,000\text{ cm}^{-1}$ , and background spectra were obtained in air.

### 2.4. Reference Assays

The seven quality indicators were measured by corresponding standard assays. A gravimetric-based loss-on-drying method was run to determine the contents of TS via hot air drying at  $105\text{ }^{\circ}\text{C}$  for 3 h. Quantitative analyses of CG, FG, DPGP, DDIFGP, AG II, and AG IV were performed using the HPLC-UV-ELSD method [19]. The flavonoids of CG, FG, DPGP, and DDIFGP were detected using UV. The saponins of AG II and AG IV were detected using ELSD.

### 2.5. Calibration Protocol

Calibration models should be developed using carefully selected and representative samples, and method development procedures need to be robust with respect to the expected variability of the products to be analyzed and the manufacturing processes used to prepare them [7]. Variations of raw materials, process parameters, and environmental temperature were introduced into the calibration sample set using a Box–Behnken design. As shown in Table 1, experiments of 29 runs (the central operating conditions were repeated 5 times) were performed to cover the different sources of variability. The concentrated supernatants of the first ethanol precipitation with TS contents of 45%, 40%, and 35% were prepared to obtain different raw materials for the second precipitation process. As illustrated in our previous study [20,21], the concentration of ethanol and the mass ratio of ethanol to concentrated raw materials were considered to be the two critical process parameters for the alcohol precipitation process. Additionally, the spectral acquisition position of each experiment was randomly set to include the different positions of the samples in the container. In the meantime of spectral acquisition, samples were collected for reference assays. Seven samples were collected for each experiment for batches 1 to 22, as shown in Table 1, and in total, 154 samples were included in the calibration set.

**Table 1.** Conditions for the alcohol precipitation experiments according to the Box–Behnken design.

Batch	TS Contents of the Concentrated Raw Materials (%)	Ethanol Concentration (%)	Mass Ratio of Ethanol to the Concentrated Raw Materials (g/g)	Temperature ( $^{\circ}\text{C}$ )	Usage
1	35	93	3.0	25	Calibration
2	45	93	3.0	25	Calibration
3	35	97	3.0	25	Calibration
4	45	97	3.0	25	Calibration
5	40	97	2.5	25	Calibration
6	40	93	3.5	25	Calibration
7	35	95	2.5	25	Calibration
8	45	95	2.5	25	Calibration
9	35	95	3.5	25	Calibration
10	45	95	3.5	25	Calibration
11	40	95	2.5	20	Calibration
12	40	93	3.5	25	Calibration
13	35	95	3.0	20	Calibration
14	45	95	3.0	20	Calibration
15	40	93	3.0	20	Calibration
16	40	97	3.0	20	Calibration
17	40	95	2.5	30	Calibration
18	40	95	3.5	30	Calibration
19	35	95	3.0	30	Calibration
20	45	95	3.0	30	Calibration
21	40	97	3.5	25	Calibration
22	40	97	3.0	30	Calibration

Table 1. Cont.

Batch	TS Contents of the Concentrated Raw Materials (%)	Ethanol Concentration (%)	Mass Ratio of Ethanol to the Concentrated Raw Materials (g/g)	Temperature (°C)	Usage
23	40	95	3.5	20	Validation and robustness evaluation
24	40	93	3.0	30	Validation and robustness evaluation
25	40	95	3.0	25	Robustness evaluation
26	40	95	3.0	25	Validation
27	40	95	3.0	25	Validation
28	40	95	3.0	25	Validation
29	40	95	3.0	25	Validation

### 2.6. Validation Protocol

Validation set 1 was constructed to optimize the calibration model. It encompassed samples collected from batches 23 to 29. Independent raw material with TS contents of 40% were used in the experiments, and 3 to 7 samples were randomly collected for each batch. Finally, 38 samples were included in external validation set 1.

Validation set 2 was constructed for a thorough validation of the in-line NIR method. Three batches with normal operating conditions for the second alcohol precipitation process were repeated and performed over three days. The position of the optical probe was fixed. One spectrum was collected every 1 min to provide real-time spectral information. Samples for reference assays were collected at 6 time points (0, 4, 8, 13, 18, and 30 min) near the probe in each validation batch to obtain 6 different content levels. Samples collected at the same time point during the 9 repeated batches were considered to have the same content levels. Finally, 54 samples (9 batches  $\times$  6 content levels) were included in validation set 2.

### 2.7. Multivariate Data Treatment

Partial least square regression (PLSR) was used to build the prediction models based on the calibration set. Appropriate pretreatments of the spectra were selected via a “trial-and-error” approach. To reduce the computational complexity, an experimental design was first set up to determine the optimal directions. The parameters for the improved algorithms were adjusted to select the best pretreatments.

Model validation consisted of traditional chemometric validation and validation using accuracy profiles. Conventional chemometric parameters were first used to obtain the global predictive capability of the established models based on validation sets 1 and 2. Then, the accuracy profiles computed based on validation set 2 were used for model assessment and thorough validation. Conventional statistical parameters, such as R, RMSEC, RMSECV, RMSEP, and the relative standard error of prediction (RSEP), were calculated to evaluate the model performance.

In validation set 2, for each content level, the average content values of the 9 samples were used as the true reference values. Due to process variation, it was not possible to obtain exactly the same contents when we repeated the 9 validation batches. Therefore, all prediction values were normalized in Equation (1) when calculating the accuracy profile for each content level [13].

$$y_{ij \text{ nor}} = \frac{\hat{y}_{ij}}{y_{ij}} \cdot \bar{y}_j \quad (1)$$

In the  $i$ th validation batch, for a sample of the  $j$ th content level,  $y_{ij \text{ norm}}$  is the normalized NIR predicted value,  $y_{ij}$  is the reference value,  $\hat{y}_{ij}$  is the NIR predicted value, and  $\bar{y}_j$  is the true reference value of the  $j$ th content level.

The TQ analyst software package (Thermo Fisher scientific, Madison, WI, USA) and ChemDataSolution chemometrics software (Dalian ChemDataSolution Information Technology Co. Ltd., Dalian, China) were used for spectral data treatments. The accuracy profiles were computed with e.noval V3.0b demo (Arlenda, Liège, Belgium).

### 3. Results and Discussion

#### 3.1. The Second Alcohol Precipitation Process and NIR Spectra

Due to the addition of ethanol, the system changed as alcohol-insoluble impurities emerged. The NIR spectra obtained under the main operating conditions are shown in Figure 2. The peak at  $6900\text{ cm}^{-1}$  is attributed to water and ethanol. The peaks at  $5200\text{--}5500\text{ cm}^{-1}$  and  $8500\text{ cm}^{-1}$  appeared after ethanol addition, which correspond to the 1st and 2nd overtones of C-H stretching in ethanol. [22] The system was clear before the critical point when the alcohol-insoluble impurities emerged. The whole system became turbid, and the spectra shifted after the critical point (at approximately 12 min). During the standing period (20–30 min) after the completion of ethanol addition, the impurities gathered and began to precipitate. The upper part of the system was clear again, and the precipitate was in the bottom part. The corresponding NIR spectra for this period became smooth, and the spectral shifts decreased. Therefore, the NIR spectra reflected the changing process state. The regions of  $5000\text{--}5095\text{ cm}^{-1}$  and  $5300\text{--}10,000\text{ cm}^{-1}$  were selected for model construction after removing the saturated absorption regions.

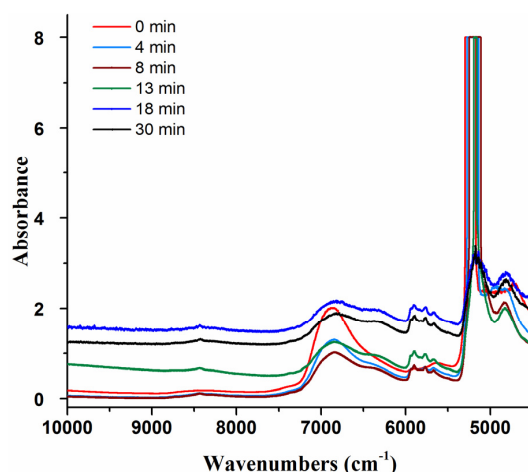


**Figure 2.** The NIR spectra during the process under normal operating conditions.

#### 3.2. Spectral Pretreatments

Different spectral pretreatments were employed to remove unwanted artifacts caused by small particles and other interference factors during the process. The typical methods used to preprocess the raw spectral data include: baseline correction, scatter correction, smoothing, and scaling [23,24]. Table 2 lists some pretreatment algorithms that are often used. Appropriate combinations of different pretreatments were selected via a “trial-and-error” approach; however, they may be computationally intensive. To reduce the number of calculations, DOE was used to determine the optimization directions. The four pretreatment steps in Table 2 were used as factors, and the full factorial design was applied to obtain 48 combinations of different pretreatments. The Norris–Williams derivation was only used to process the first or second derivation spectra. The combinations were used to process the spectra, and 48 PLSR models were obtained. The models with better performance were selected compared to the model constructed from the raw data without any pretreatments. Using the TS contents as an example, the potential optimal combinations are listed in Table 3.

Next, predictive performance and model complexity were used as evaluation indices to further optimize the parameters of the pretreatment algorithms shown in Table 3. As a result, there were a total of 80 models constructed, as included in Figure 3. Take the red triangle as reference, which represents the model built from raw data. The performances of the models in the lower left part were improved by the pretreatments. Finally, the best pretreatments that yielded a simple model with the best predictive performance were chosen. For the seven analytes, the best pretreatment combinations are listed in Table 4.

**Table 2.** Overview of some commonly used algorithms for each pretreatment method.

Baseline Correction	Scatter Correction	Smoothing	Scaling
-	-	-	Mean centering
1st D <sup>a</sup>	MSC <sup>c</sup>	SG <sup>e</sup>	Auto scaling
2nd D <sup>b</sup>	SNV <sup>d</sup>	NW <sup>f</sup>	

<sup>a</sup> First derivation (1st D). <sup>b</sup> Second derivation (2nd D). <sup>c</sup> Multiplicative scatter correction (MSC). <sup>d</sup> Standard normal variate (SNV). <sup>e</sup> Savitzky–Golay polynomial derivative filter (SG) using a 9-point window and a third-order polynomial as the initial default parameters. <sup>f</sup> Norris–Williams derivation (NW) using 5-point smoothing and a gap size of 5 as the initial default parameters.

**Table 3.** Potential optimal pretreatment combinations for the TS content models.

Baseline Correction	Scatter Correction	Smoothing	Scaling	LVs <sup>a</sup>	Calibration Set		Validation Set 1	
					R <sub>C</sub>	RMSEC	R <sub>P</sub>	RMSEP
-	-	-	Auto scaling	6	0.9783	2.28	0.9954	1.07
-	MSC	-	Auto scaling	6	0.9692	2.71	0.9954	1.03
-	MSC	SG	Auto scaling	5	0.9622	3.00	0.9939	1.18
1st D	-	NW	Auto scaling	3	0.9651	2.88	0.9950	1.06
1st D	-	SG	Auto scaling	7	0.9861	1.83	0.9950	1.23
2nd D	-	NW	Auto scaling	4	0.9768	2.36	0.9963	0.83

<sup>a</sup> The number of latent variables (LVs) reveals the complexity of the models.

**Table 4.** Performance parameters of the seven calibration models.

Analytes	Pretreatment Combinations	LVs	Calibration Set		Cross-Validation		Validation Set 1	
			R <sub>C</sub>	RMSEC	R <sub>CV</sub>	RMSECV	R <sub>P</sub>	RMSEP
TS	NW <sup>a</sup> + 2nd D + auto scaling	3	0.9711	2.63%	0.9602	3.11%	0.9974	0.74%
CG	SG <sup>b</sup> + 1st D + auto scaling	3	0.9614	0.169 mg/mL	0.9504	0.192 mg/mL	0.9963	0.0460 mg/mL
FG	NW <sup>a</sup> + 2nd D + auto scaling	3	0.971	0.0316 mg/mL	0.9549	0.0395 mg/mL	0.9924	0.0142 mg/mL
DPGP	NW <sup>a</sup> + 2nd D + auto scaling	3	0.9691	0.0629 mg/mL	0.9522	0.0784 mg/mL	0.9967	0.0197 mg/mL
DDIFGP	NW <sup>c</sup> + 1st D + auto scaling	3	0.9621	0.0256 mg/mL	0.9517	0.0289 mg/mL	0.9941	0.00865 mg/mL
AG II	SG <sup>e</sup> + mean centering	6	0.9675	0.0601 mg/mL	0.9618	0.0652 mg/mL	0.9656	0.0841 mg/mL
AG IV	NW <sup>d</sup> + 1st D + auto scaling	3	0.9416	0.0590 mg/mL	0.9268	0.0659 mg/mL	0.9762	0.0325 mg/mL

<sup>a</sup> NW using a 7-point smoothing and a gap size of 7. <sup>b</sup> SG using an 11-point window and a second-order polynomial. <sup>c</sup> NW using a 3-point smoothing and a gap size of 5. <sup>d</sup> NW using a 5-point smoothing and a gap size of 3. <sup>e</sup> SG using a 9-point window and a third-order polynomial.

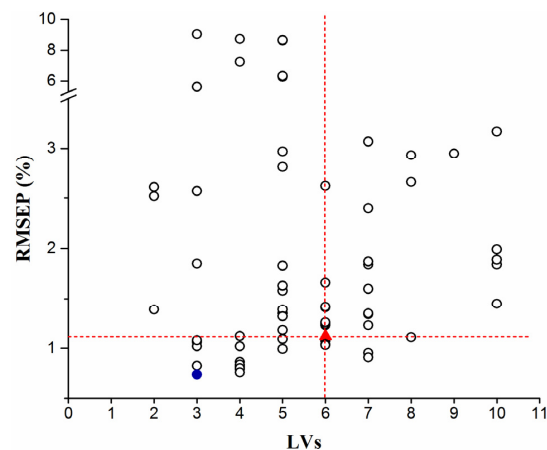


**Figure 3.** Overview of the TS content models for all pretreatment combinations. (The red triangle represents the model built from raw data, and the blue dot represents the final model built from the best pretreatments).

### 3.3. Development of Calibration Models

A four-fold cross-validation was used to choose the number of LVs for each PLSR model. The quantitative models were constructed for NIR spectra and the seven analytes. The conventional statistical parameters, such as R of calibration ( $R_C$ ), R of cross-validation ( $R_{CV}$ ), R of prediction ( $R_P$ ), RMSEC, RMSECV, and RMSEP, were calculated to evaluate the model performance. The detailed performance parameters of the seven models are summarized in Table 4. The obtained models have a small number of LVs, which limit the risk of overfitting. Promising results in terms of high correlation coefficients and low prediction errors were obtained. Figure 4 shows the correlation plots of reference values versus the NIR predictions for the seven analytes. The plots present the fitting and predictive ability of the seven models for the entire content range. The models demonstrate good global predictive performance for the seven analytes of the target process samples in the external validation set 1.

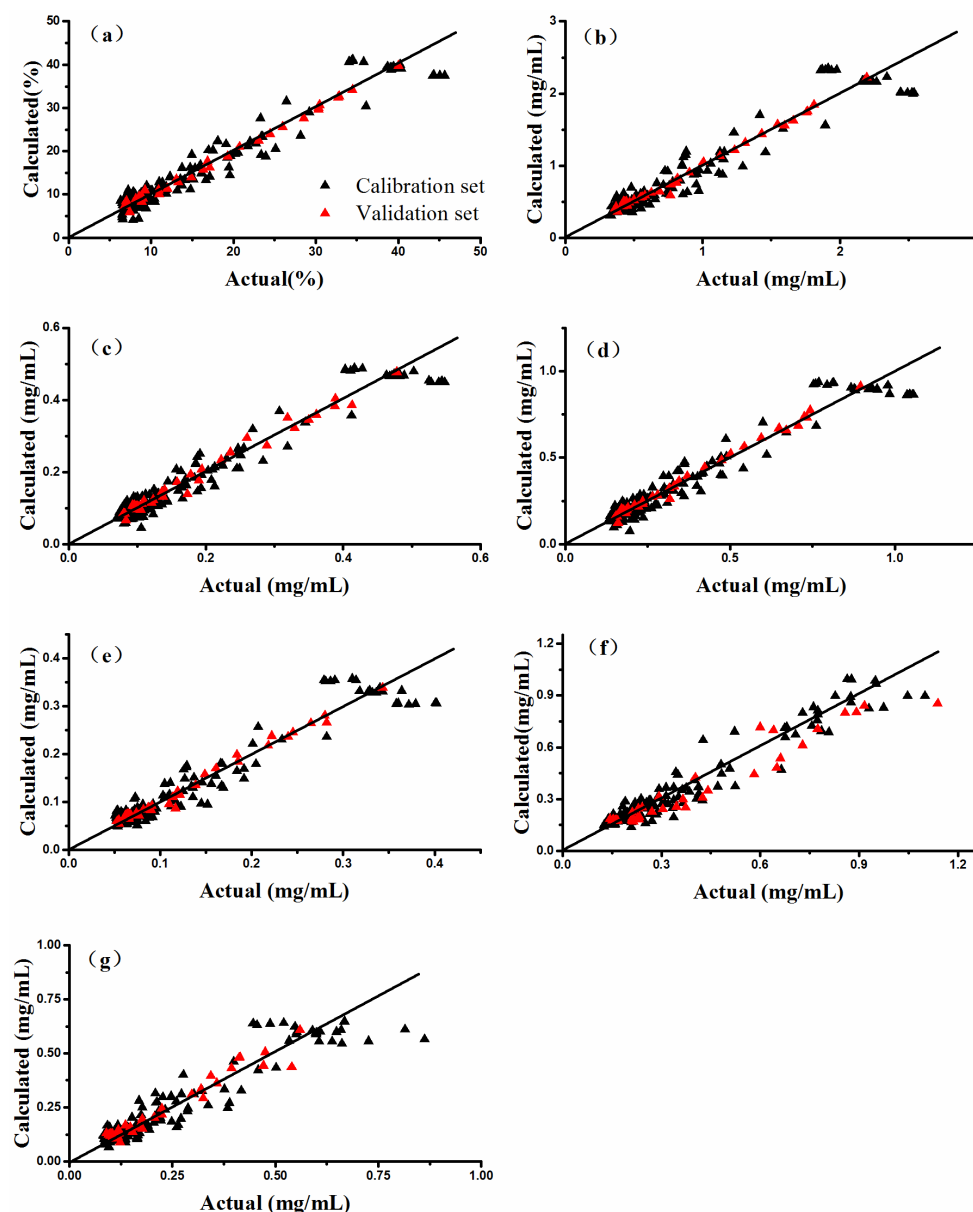


**Figure 4.** Correlation plots for reference values versus NIR predictions for the PLSR models of TS (a), CG (b), FG (c), DPGP (d), DDIFGP (e), AG II (f), and AG IV (g).

### 3.4. In-Line Monitoring of the Second Alcohol Precipitation Process and Chemometric Validation

The established calibration models were used to predict the contents of the seven analytes during the second alcohol precipitation process under normal operating conditions. Figure 5 shows the in-line monitoring results of nine alcohol precipitation batches. To further evaluate the model performance, 54 samples in validation set 2 were collected for reference assays from the nine batches. The newly added parameter of RSEP together with RMSEP and R were used to evaluate the different aspects of the model quality. Table 5 shows the chemometric validation parameters of the quantitative models for the seven analytes. The results demonstrate that the models still present a good overall predictive performance for the samples in the independent new batches. Compared with the parameters in Table 4, the difference in RMSEP values is low. In addition, the first four models for TS, CG, FG, and DPGP perform better than the models for DDIFGP, AG II, and AG IV regarding the RSEP values.

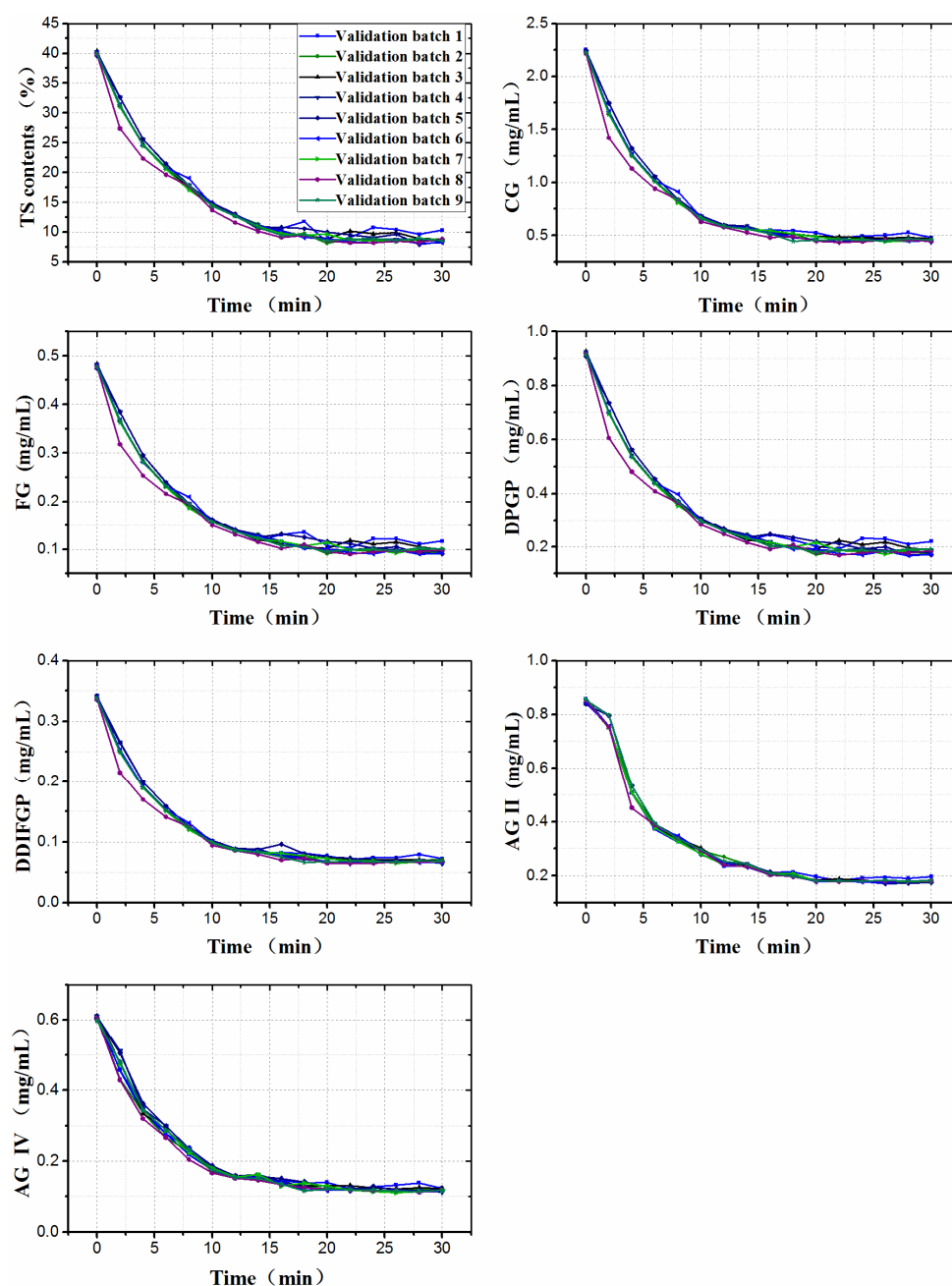


Figure 5. In-line monitoring results of 9 validation batches of the second alcohol precipitation.

**Table 5.** Chemometric validation parameters for the 7 quantitative models.

Analytes	Validation Set 2		
	R	RMSEP	RSEP
TS	0.9988	0.53%	2.41%
CG	0.9977	0.0437 mg/mL	3.73%
FG	0.9961	0.0126 mg/mL	4.79%
DPGP	0.9972	0.0199 mg/mL	4.10%
DDIFGP	0.9748	0.0253 mg/mL	13.4%
AG II	0.9331	0.0766 mg/mL	15.6%
AG IV	0.9864	0.0256 mg/mL	8.58%

3.5. Validation Based on Accuracy Profiles

The accuracy profile approach using the concept of total error (bias and standard deviation) is fully compliant with the ICH Q2(R1) requirements in which different validation characteristics should be considered. The following sections discuss in detail the validation criteria for the established models.

3.5.1. Trueness

Trueness represents the systematic error in the measurements. It refers to the closeness in agreement between the average of the measured results and the accepted reference value [25,26]. Trueness is generally expressed in terms of relative bias and recovery.

The calculated results of the six different content levels for each analyte are listed in Tables 6 and 7. All seven models exhibited a higher relative bias as a function of increasing content. The relative bias became much higher for the lower content range of 0.246–0.386 mg/mL for the AG II model, and for the other six models shown in Table 8, all values were within 12.5%. Most values fell within 5%.

**Table 6.** Validation criteria of trueness, precision, and accuracy of the models for the 7 analytes.

Analytes	Content Level	Trueness		Precision		Accuracy
		Relative Bias (%)	Relative Bias (%)	Repeatability (RSD%)	Intermediate Precision (RSD%)	Relative $\beta$ -Expectation Tolerance Limits (%)
TS (%)	39.8	0.43	100.4	0.34	0.92	[−3.40, 4.25]
	25.0	−1.66	98.34	0.81	0.81	[−3.64, 0.33]
	17.9	−0.84	99.16	3.2	3.2	[−8.65, 6.97]
	12.7	−6.17	93.83	2.2	2.5	[−12.86, 0.53]
	9.4	1.65	101.7	5.4	5.4	[−11.58, 14.88]
	8.4	3.81	103.8	2.1	3.2	[−9.04, 10.99]
CG (mg/mL)	2.26	−1.47	98.53	2.2	2.8	[−9.63, 6.68]
	1.27	−0.85	99.15	1.4	1.4	[−4.29, 2.59]
	0.853	−2.18	97.82	3.9	4.0	[−12.02, 7.67]
	0.591	−1.37	98.63	1.4	2.7	[−11.31, 8.58]
	0.461	8.95	109.0	5.9	6.3	[−7.32, 25.23]
	0.408	12.31	112.3	2.2	3.2	[2.35, 22.27]
FG (mg/mL)	0.502	−4.51	95.49	0.86	1.5	[−9.57, 0.55]
	0.291	−3.03	96.97	1.5	1.5	[−6.60, 0.53]
	0.195	−0.37	99.63	3.6	3.9	[−10.33, 9.58]
	0.137	−3.18	96.82	1.9	2.0	[−8.26, 1.91]
	0.104	6.16	106.2	7.7	7.7	[−12.61, 24.92]
	0.091	8.59	108.6	7.7	8.9	[−14.86, 32.04]
DPGP (mg/mL)	0.939	−2.27	97.73	2.1	2.1	[−7.29, 2.74]
	0.525	2.36	102.4	1.7	2.4	[−5.09, 9.80]
	0.360	1.93	101.9	3.8	4.0	[−8.09, 11.96]
	0.246	−0.46	99.54	2.1	2.1	[−5.68, 4.75]
	0.189	8.55	108.6	7.5	7.5	[−9.75, 26.85]
	0.167	11.14	111.1	8.6	10	[−15.94, 38.22]

**Table 7.** Validation criteria of trueness, precision, and accuracy of the models for the 7 analytes.

Analytes	Content Level	Trueness		Precision		Accuracy
		Relative Bias (%)	Relative Bias (%)	Repeatability (RSD%)	Intermediate Precision (RSD%)	Relative $\beta$ -Expectation Tolerance limits (%)
DDIFGP (mg/mL)	0.384	-10.55	89.45	9.2	9.2	[-33.10, 12.01]
	0.188	1.42	101.42	2.4	4.3	[-14.01, 16.85]
	0.121	2.51	102.5	3.0	3.3	[-5.83, 10.86]
	0.0847	3.28	103.3	3.6	5.6	[-14.69, 21.24]
	0.0701	7.53	107.5	8.9	12	[-29.41, 44.48]
	0.0633	8.01	108.0	4.2	6.6	[-13.49, 29.51]
AG II (mg/mL)	0.879	-3.15	96.85	2.0	3.4	[-14.60, 8.29]
	0.509	0.17	100.2	2.2	2.8	[-7.75, 8.08]
	0.346	-2.77	97.23	2.3	2.3	[-8.47, 2.92]
	0.386	-38.53	61.47	1.8	1.8	[-42.95, 34.11]
	0.284	-29.14	70.86	2.8	2.8	[-35.98, -22.30]
	0.246	-26.16	73.84	2.1	2.8	[-34.13, -18.19]
AG IV (mg/mL)	0.556	9.53	109.5	4.7	4.7	[-1.867, 20.93]
	0.336	1.72	101.7	3.4	4.9	[-13.44, 16.88]
	0.235	-2.14	97.9	2.3	2.7	[-9.11, 4.84]
	0.167	-6.37	93.6	2.8	2.8	[-13.21, 0.48]
	0.124	4.62	104.6	6.7	6.7	[-11.75, 20.99]
	0.106	12.08	112.1	4.0	8.3	[-19.33, 43.49]

**Table 8.** The valid range for each analyte and its proportion over the studied content range.

Analytes	LLOQ–ULOQ	Proportion (%)
TS	8.44–39.8%	100
CG	0.541–2.26 mg/mL	93.1
FG	0.118–0.502 mg/mL	93.5
DPGP	0.220–0.940 mg/mL	93.3
DDIFGP	0.106–0.167 mg/mL	18.9
AG II	0.484–0.879 mg/mL	62.4
AG IV	0.137–0.320 mg/mL	40.8

### 3.5.2. Precision

Precision represents the random error in the measurements. It refers to the closeness in agreement between a series of measurements of the same homogeneous sample obtained under various conditions [25]. Precision is evaluated at two levels: repeatability and intermediate precision, and the results are listed in Tables 6 and 7. The relative standard deviation (RSD%) shows good precision at high content levels for the seven analytes, whereas at low content levels, some random errors were observed. Of the seven models, the AG II model was the most precise model.

### 3.5.3. Accuracy

Accuracy expresses the closeness in agreement between a single measured result and the accepted reference value [25], and it represents the total measurement error, which is the sum of the trueness and precision. The accuracy at different content levels for the seven analytes calculated at the relative 95%  $\beta$ -expectation tolerance limits are shown in Tables 6 and 7. The obtained intervals produced error ranges that suggested that the future NIR predicted results will fall within a 95% probability. The accuracy profile was built by integrating the total error and the calculated tolerance limits at each content level in one plot, as shown in Figure 6. These profiles constitute a visual decision tool when compared with the predefined acceptance limits. The acceptance limits for the in-line determination of the seven analytes were fixed at 15%, and the NIR quantitative method was considered to be valid when the relative errors of the predicted values were within 15% of the studied content range. As shown in Figure 6, for the first four analytes, the relative  $\beta$ -expectation tolerance limits for most content levels were included within the acceptance limit of  $\pm 15\%$ . For the last three analytes, the accuracy did not fulfill the acceptance limits for some content levels, especially for lower levels.

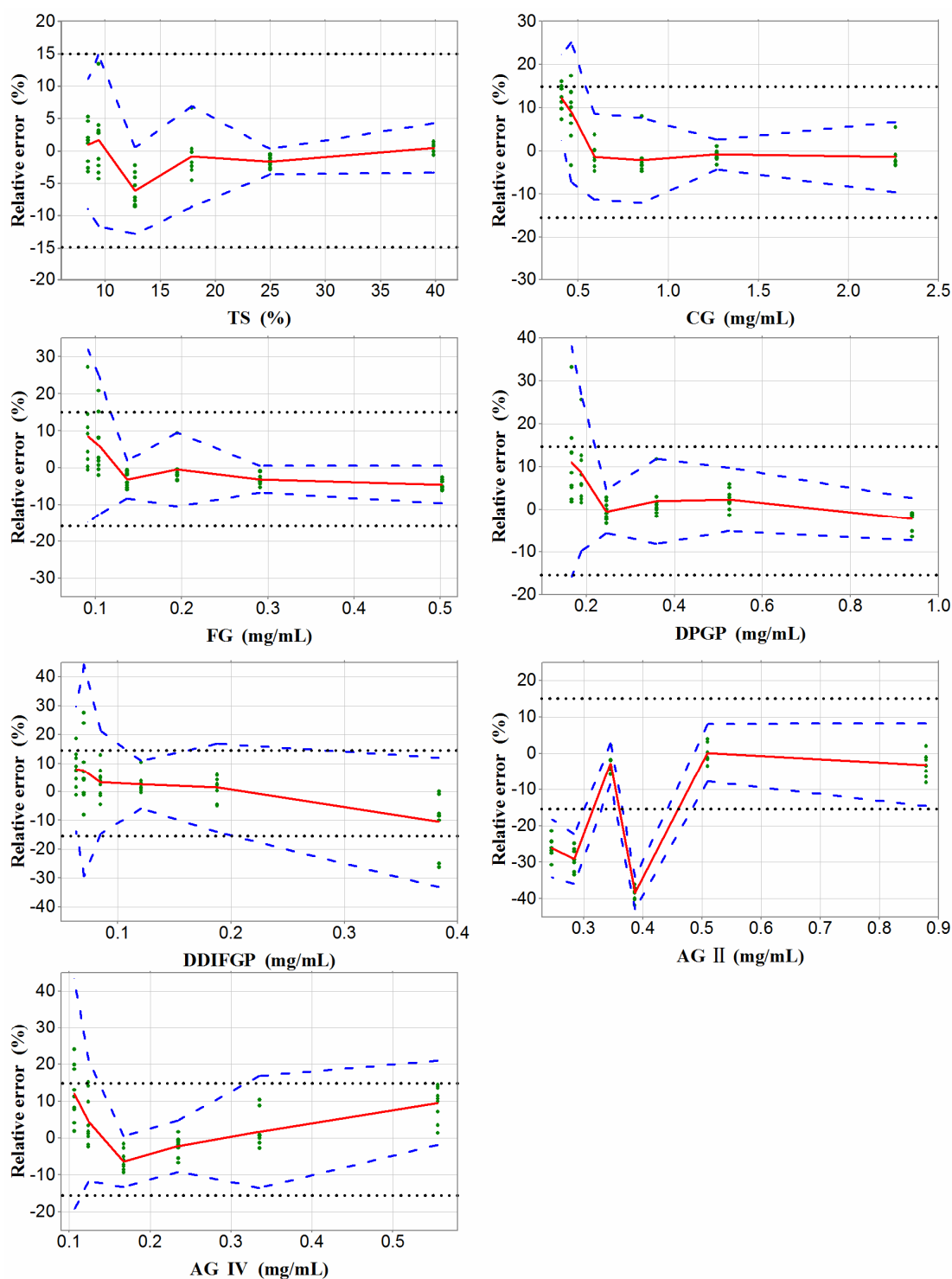


**Figure 6.** Accuracy profiles for the 7 PLSR models. (The plain red line represents the relative bias, the dashed blue lines represent the  $\beta$ -expectations tolerance limits ( $\beta = 95\%$ ), and the dotted black lines represent the acceptance limits ( $\pm 15\%$ )).

### 3.5.4. Linearity

The linearity of an analytical procedure is its ability within a definite range to obtain results that are directly proportional to the amount of the analyte in the sample [24]. Figure 7 presents the linear profiles of the seven models with  $R^2$  values and the linear equations. The  $R^2$  values are larger than 0.95, which indicate the overall high linearity of the models. The intercepts in the equations are close to 0, confirming the absence of a constant systematic

error, and all slopes are close to 1 in the equations except the slope for DDIFGP, which indicates a certain proportional systematic error in that quantification model. However, the method can be considered linear within the content range where the  $\beta$ -expectation tolerance limits are within the absolute acceptance limits.

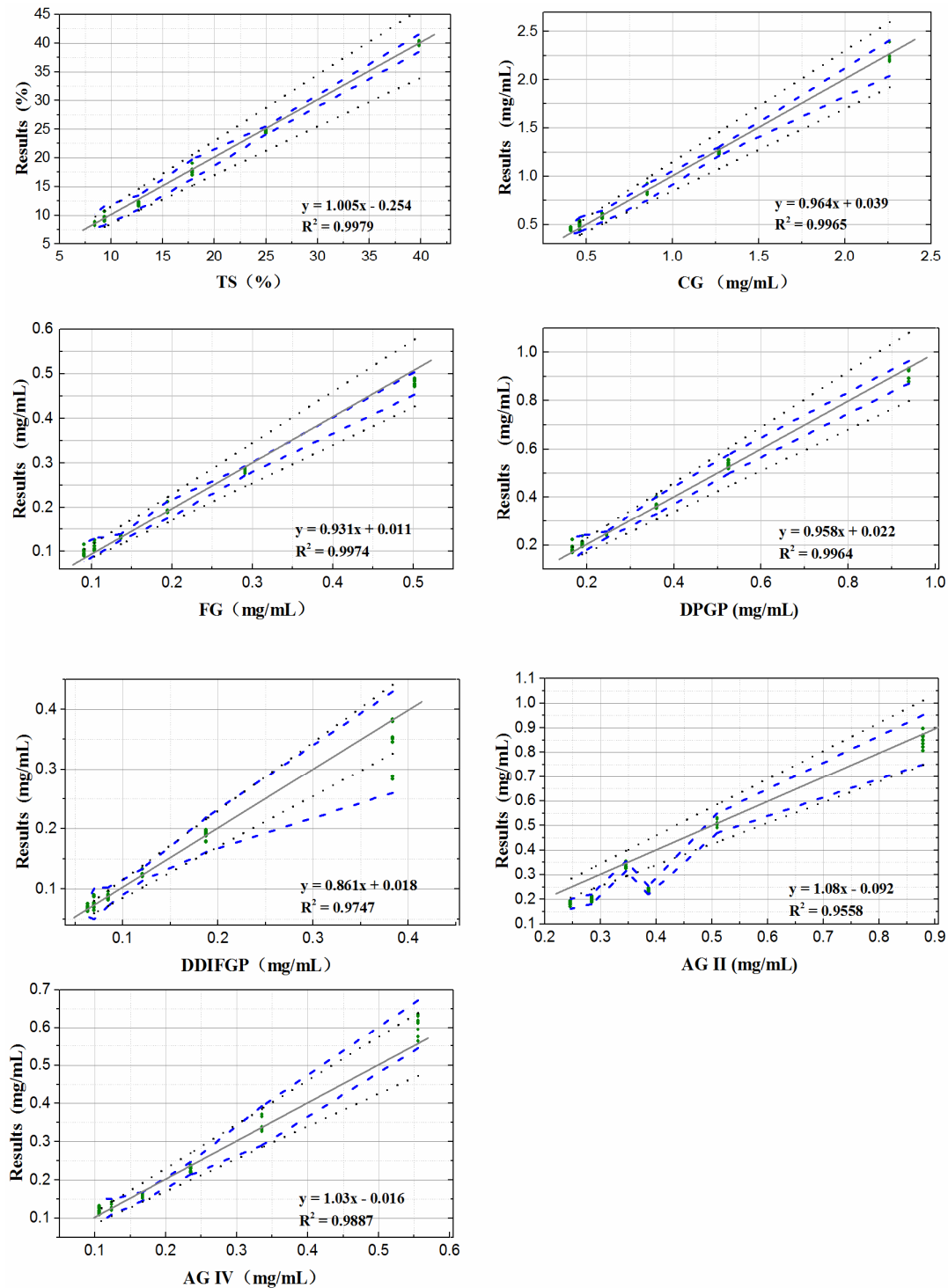


**Figure 7.** Linear profiles for the 7 PLSR models. (The dashed blue lines on this graph correspond to the accuracy profiles, i.e., the  $\beta$ -expectations tolerance limits expressed in absolute values. The dotted black lines represent the acceptance limits at  $\pm 15\%$  expressed in concentration units. The solid line is the identity line for  $y = x$ ).

### 3.5.5. Range

The range of an analytical procedure is the interval between the upper and lower amounts of analyte in a sample for which it has been demonstrated that the analytical procedure has a suitable level of precision, accuracy, and linearity [26]. According to Figure 6, the range between the lower and upper limits of quantification can be obtained where the relative  $\beta$ -expectation tolerance limits are included within the acceptance limits. The range for each quantification model is listed in Table 8. For the first four analytes, the established NIR models were able to predict accurate results over more than 90% of the content range for the second alcohol precipitation process. However, for the last three models, accurate results could be guaranteed within the higher content ranges for the process. Of the seven analytes, the content of DDIFGP was the lowest in the samples, which may be close to the sensitivity limit of the NIR spectrometer, which may be prone to large prediction errors. For AG II and AG IV, as the HPLC-ELSD method was applied as the reference quantitative method, which is less accurate than the HPLC-UV method, the prediction models yielded narrower valid ranges than the three models for CG, FG, and DPGP. Moreover, the complexity of the changing system during the in-line analysis and the existence of the alcohol-insoluble impurities made it more difficult to obtain more accurate models.

### 3.5.6. Robustness

The robustness of an analytical procedure is a measure of its capacity to remain unaffected by small but deliberate variations in the method parameters during normal usage [26]. At the stage of method development, the expected variability was built into the calibration set by DOE, and the obtained models had a small number of LVs, which characterized their robustness. At the stage of validation, stable RMSEP values calculated from two independent validation sets were obtained for the seven models, which indicated the robustness. To further evaluate method robustness, critical process parameters, and temperature were deliberately altered. As listed in Table 1, batch 23 and 24 were selected, and seven samples were randomly collected from each batch. The content results of the seven analytes in the samples were compared and are shown in Figure 8, which were obtained via the off-line reference methods and in-line NIR analysis. The established NIR spectroscopy method retained good in-process performance even with deliberate process variations.

### 3.5.7. Specificity

The specificity refers to the ability to unequivocally assess an analyte in the presence of components that are expected to be present [26]. The NIR spectrum is characterized by wide and overlapping absorption bands, and it is quite difficult to assign a value to a specific chemical component because of the complexity of TCMs. The specificity of the models was demonstrated by the variance in the reference data that was covered by the LVs [27]. Three LVs were used for quantitative models of TS, CG, FG, DPGP, DDIFGP, and AG IV, explaining 94.3%, 92.9%, 94.3%, 93.9%, 92.6%, and 88.7% of the total variance in the data, respectively. Six LVs were used for quantitative models of AG II, explaining 93.6% of the total variance in the data. This result indicated that each model contained enough content information of the target analyte and demonstrated the specificity [28].

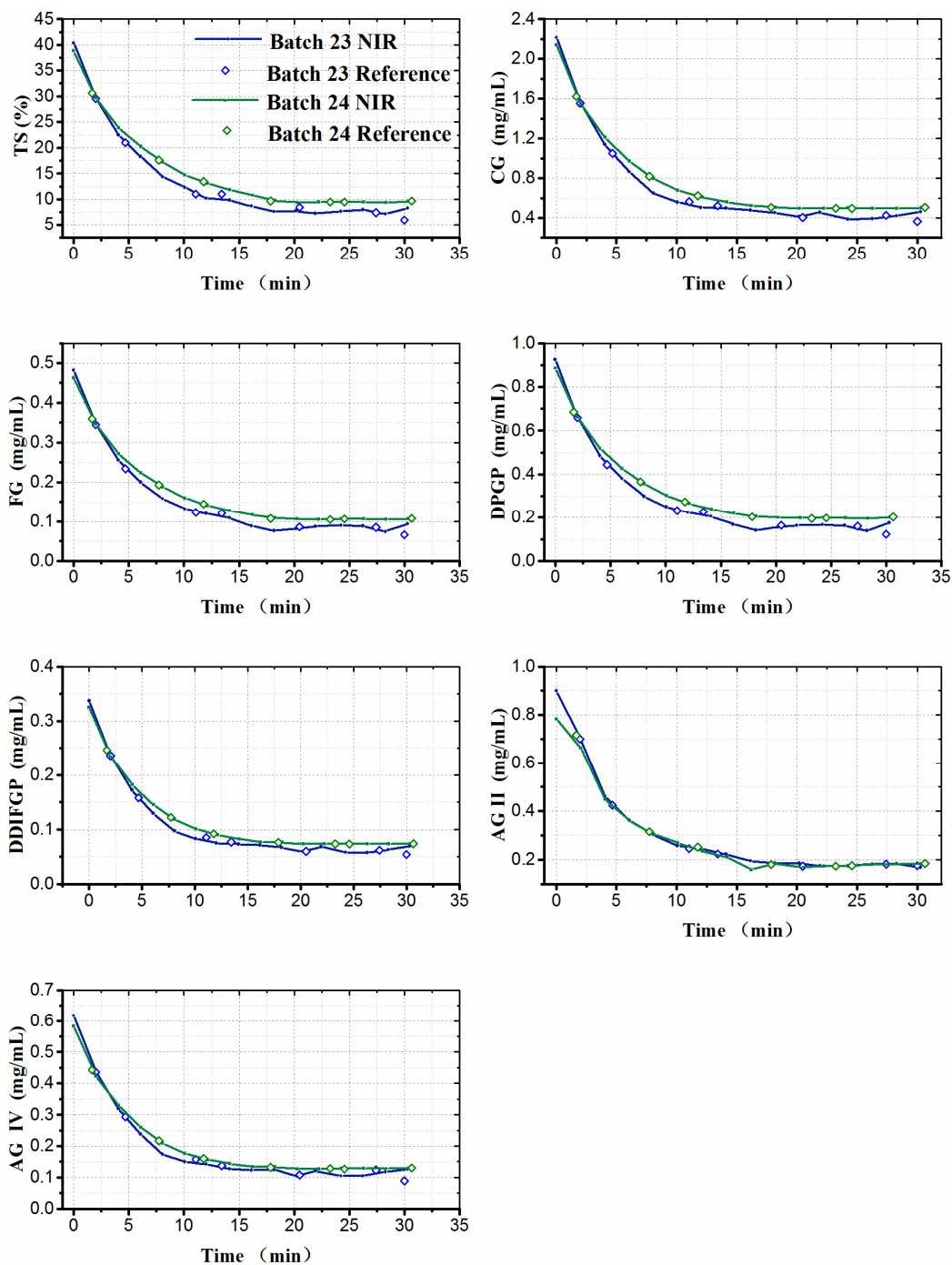


**Figure 8.** Robustness of the in-line NIR spectroscopy method. (In-line monitoring results are shown as the lines, where the results of the randomly collected 7 samples were obtained via off-line reference methods).

### 3.6. Method Uncertainty Assessment

The uncertainty characterizes the dispersion of the values that can reasonably be attributed to the measurement [29]. The uncertainties in the bias of the NIR spectroscopy method at each content level for the seven analytes are displayed in Tables 9 and 10. The expanded uncertainty refers to an interval around the results where an unknown true value can be observed with a confidence level of 95% [30], and the relative expanded uncertainties obtained by dividing the expanded uncertainties with the corresponding true reference content values were not higher than 11.5% over the entire TC validated range, which means that at a confidence level of 95%, the unknown true value is located at a maximum of ±

11.5% around the NIR result. For the other six analytes, the relative expanded uncertainties did not exceed 8.5%, 8.6%, 8.6%, 13.0%, 11.0%, or 7.6% over the respective valid ranges between the lower and upper limits of quantification.

**Table 9.** NIR method uncertainties for the 7 analytes.

Analytes	Content Level	Uncertainty	Expanded Uncertainty	Relative Expanded Uncertainty (%)
TS (%)	39.8	0.42	0.83	2.1
	25.0	0.21	0.43	1.7
	17.9	0.6	1.2	6.7
	12.7	0.35	0.70	5.5
	9.4	0.54	1.1	11.4
	8.4	0.30	0.60	7.1
CG (mg/mL)	2.26	0.071	0.14	6.3
	1.27	0.019	0.038	3.0
	0.853	0.036	0.072	8.4
	0.591	0.018	0.036	6.2
	0.461	0.031	0.063	13.6
	0.408	0.015	0.029	7.1
FG (mg/mL)	0.502	0.0083	0.017	3.32
	0.291	0.0045	0.0089	3.1
	0.195	0.0082	0.016	8.4
	0.137	0.003	0.0059	4.3
	0.104	0.0084	0.017	16.2
	0.091	0.0087	0.017	19.2
DPGP (mg/mL)	0.939	0.020	0.041	4.3
	0.525	0.014	0.028	5.4
	0.360	0.015	0.031	8.52
	0.246	0.0055	0.011	4.5
	0.189	0.015	0.030	15.8
	0.167	0.018	0.037	21.9

**Table 10.** NIR method uncertainties for the 7 analytes.

Analytes	Content Level	Uncertainty	Expanded Uncertainty	Relative Expanded Uncertainty (%)
DDIFGP (mg/mL)	0.384	0.037	0.075	19.4
	0.188	0.0092	0.018	9.8
	0.121	0.0042	0.0085	7.0
	0.0847	0.0053	0.011	12.4
	0.0701	0.0096	0.019	27.3
	0.0633	0.0047	0.0093	14.7
AG II (mg/mL)	0.879	0.034	0.067	7.6
	0.509	0.016	0.031	6.1
	0.346	0.0085	0.017	4.9
	0.386	0.0074	0.015	3.8
	0.284	0.0084	0.017	5.9
	0.246	0.0075	0.015	6.1
AG IV (mg/mL)	0.556	0.027	0.055	9.8
	0.336	0.018	0.037	11.0
	0.235	0.0067	0.013	5.7
	0.167	0.0049	0.010	5.9
	0.124	0.0087	0.017	14.1
	0.106	0.010	0.020	18.8

#### 4. Conclusions

This study explored an in-line NIR spectroscopy method for multicomponent quantification during the second alcohol precipitation process of *Astragali radix*.

At the stage of method development, a calibration set that encompassed enough variation was built, and models were optimized using the DOEs, reducing the calculation times via a trial-and error approach. Finally, the established PLS models had a small number of LVs, and promising results in terms of high correlation coefficients and low prediction errors were obtained.

At the validation stage, traditional chemometric validation and the accurate profile approach were compared. The general good predictive capability of the seven models was demonstrated using the conventional statistical parameters, and the models were further validated using accuracy profiles. According to the predefined acceptance limits, the accuracy profiles produced a reliable representation of the future performances of the NIR spectroscopy method. A visual decision tool to select valid content ranges showed the following results: 8.44–39.8%, 0.541–2.26 mg/mL, 0.118–0.502 mg/mL, 0.220–0.940 mg/mL, 0.106–0.167 mg/mL, 0.484–0.879 mg/mL, and 0.137–0.320 mg/mL for TS, CG, FG, DPGP, DDIFGP, AG II, and AG IV, respectively. Generally, the developed NIR spectroscopy method can be applied for in-line prediction of the early and middle stage of the second alcohol precipitation process. Additionally, the validation results demonstrated acceptable trueness, precision, accuracy, linearity, specificity, and robustness over the ranges, which were in compliance with the ICH Q2(R1) guideline.

**Author Contributions:** Conceptualization, W.L., Y.L. and X.W.; methodology, Y.L. and X.W.; software, X.W. and Y.L.; validation, Y.L., X.W. and X.G.; formal analysis, W.L., X.G. and H.Q.; investigation, W.L. and H.Q.; resources, W.H. and G.W.; data curation, W.L., Y.L. and X.W.; writing—original draft preparation, W.L., Y.L. and H.Q.; writing—review and editing, W.L., Y.L., W.H., G.W. and H.Q.; visualization, W.L., X.G. and W.H.; supervision, W.L. and H.Q.; project administration, W.H., G.W. and H.Q.; funding acquisition, W.H. and G.W. All authors have read and agreed to the published version of the manuscript.

**Funding:** This research was funded by [Xingchu Gong] the National Project for Standardization of Chinese Materia Medica (ZYBZH-C-GD-04), and [Wenlong Li] the Key Project from the National Project for Standardization of Chinese Materia Medica (ZYBZH-C-JIN-43).

**Data Availability Statement:** Data are contained within the article.

**Conflicts of Interest:** The authors declare no conflict of interest.

## References

1. Li, S.Y.; Wang, D.; Li, X.R.; Qin, X.M.; Du, Y.G.; Li, K. Identification and activity evaluation of Astragalus Radix from different germplasm resources based on specific oligosaccharide fragments. *Chin. Herb. Med.* **2021**, *13*, 33–42. [[CrossRef](#)] [[PubMed](#)]
2. Cao, S.N.; Hou, G.J.; Meng, Y.; Chen, Y.; Xie, L.; Shi, B. Network Pharmacology and Molecular Docking-Based Investigation of Potential Targets of Astragalus membranaceus and Angelica sinensis Compound Acting on Spinal Cord Injury. *Dis. Mark.* **2022**, *2022*, 2141882. [[CrossRef](#)] [[PubMed](#)]
3. Gong, F.Y.; Qu, R.M.; Li, Y.C.; Lv, Y.; Dai, J. Astragalus Mongholicus: A review of its anti-fibrosis properties. *Front. Pharm.* **2022**, *13*, 976561. [[CrossRef](#)] [[PubMed](#)]
4. Gong, X.C.; Wang, S.; Li, Y.; Qu, H.B. Separation characteristics of ethanol precipitation for the purification of the water extract of medicinal plants. *Sep. Purif. Technol.* **2013**, *107*, 273–280. [[CrossRef](#)]
5. Liang, X.L.; Ji, M.M.; Chen, L.; Liao, Y.; Kong, X.Q.; Xu, X.Q.; Liao, Z.G.; Wilson, W.D. Traditional Chinese herbal medicine Astragalus Radix and its effects on intestinal absorption of aconite alkaloids in rats. *Chin. Herb. Med.* **2021**, *13*, 235–242. [[CrossRef](#)] [[PubMed](#)]
6. Zheng, H.; Dong, Z.; Shr, Q. *Modern Study of Traditional Chinese Medicine*; Xue Yuan Press: Beijing, China, 1998; Volume 4, p. 3886.
7. European Medicines Agency (EMA). *Guideline on the Use of Near Infrared Spectroscopy by the Pharmaceutical Industry and the Data Requirements for New Submissions and Variations*; EMA: Amsterdam, The Netherlands, 2014.
8. Engel, J.; Gerretzen, J.; Szymanska, E.; Jansen, J.J.; Downey, G.; Blanchet, L.; Buydens, L.M.C. Breaking with trends in pre-processing? *TrAC Trends Anal. Chem.* **2013**, *50*, 96–106. [[CrossRef](#)]
9. *International Conference on Harmonisation (ICH) of Technical Requirements for Registration of Pharmaceuticals for Human Use, Tpoic Q2 (A), Test on Validation of Analytical Procedures*; ICH: Geneva, Switzerland, 1994.
10. Bleye, C.; Chavez, P.F.; Mantanus, J.; Marini, R.; Hubert, P.; Rozet, E.; Ziemons, E. Critical review of near-infrared spectroscopic methods validations in pharmaceutical applications. *J. Pharm. Biomed.* **2012**, *69*, 125–132. [[CrossRef](#)] [[PubMed](#)]

11. Kauppinen, A.; Toiviainen, M.; Lehtonen, M.; Jarvinen, K.; Paaso, J.; Juuti, M.; Ketolainen, J. Validation of a multipoint near-infrared spectroscopy method for in-line moisture content analysis during freeze-drying. *J. Pharm. Biomed.* **2014**, *95*, 229–237. [[CrossRef](#)] [[PubMed](#)]
12. Schaefer, C.; Clicq, D.; Lecomte, C.; Merschaert, A.; Norrant, E.; Fotiad, F. A Process Analytical Technology (PAT) approach to control a new API manufacturing process: Development, validation and implementation. *Talanta* **2014**, *120*, 114–125. [[CrossRef](#)] [[PubMed](#)]
13. Fonteyne, M.; Arruabarrena, J.; Beer, J.; Hellings, M.; Kerkhof, T.V.; Burggraeve, A.; Vervaet, C.; Remon, J.P.; Beer, T. NIR spectroscopic method for the in-line moisture assessment during drying in a six-segmented fluid bed dryer of a continuous tablet production line: Validation of quantifying abilities and uncertainty assessment. *J. Pharm. Biomed.* **2014**, *100*, 21–27. [[CrossRef](#)] [[PubMed](#)]
14. Sun, M.F.; Yang, J.Y.; Cao, W.; Shao, J.Y.; Wang, G.X.; Qu, H.B.; Huang, W.H.; Gong, X.C. Critical process parameter identification of manufacturing processes of *Astragali radix* extract with a weighted determination coefficient method. *Chin. Herb. Med.* **2020**, *12*, 125–132. [[CrossRef](#)] [[PubMed](#)]
15. Hubert, P.; Nguyen-Huu, J.J.; Boulanger, B.; Chapuzet, E.; Chiap, P.; Cohen, N.; Compagnon, P.A.; Dewe, W.; Feinberg, M.; Lallier, M.; et al. Harmonization of strategies for the validation of quantitative analytical procedures—A SFSTP proposal—Part II. *J. Pharm. Biomed.* **2007**, *45*, 70–81. [[CrossRef](#)] [[PubMed](#)]
16. Hubert, P.; Nguyen-Huu, J.J.; Boulanger, B.; Chapuzet, E.; Cohen, N.; Compagnon, P.A.; Dewe, W.; Feinberg, M.; Laurentie, M.; Mercier, N.; et al. Harmonization of strategies for the validation of quantitative analytical procedures—A SFSTP proposal—Part III. *J. Pharm. Biomed.* **2007**, *45*, 82–96. [[CrossRef](#)] [[PubMed](#)]
17. Hubert, P.; Nguyen-Huu, J.J.; Boulanger, B.; Chapuzet, E.; Cohen, N.; Compagnon, P.A.; Dewe, W.; Feinberg, M.; Laurentie, M.; Mercier, N.; et al. Harmonization of strategies for the validation of quantitative analytical procedures: A SFSTP proposal Part IV. Examples of application. *J. Pharm. Biomed.* **2008**, *48*, 760–771. [[CrossRef](#)]
18. Wu, Z.; Ma, Q.; Lin, Z.; Peng, Y.; Ai, L.; Shi, X.; Qiao, Y. A novel model selection strategy using total error concept. *Talanta* **2013**, *107*, 248–254. [[CrossRef](#)]
19. Wu, Z.; Xu, B.; Du, M.; Sui, C.; Shi, X.; Qiao, Y. Validation of a NIR quantification method for the determination of chlorogenic acid in *Lonicera japonica* solution in ethanol precipitation process. *J. Pharm. Biomed.* **2012**, *62*, 1–6. [[CrossRef](#)] [[PubMed](#)]
20. Xue, Z.; Xu, B.; Yang, C.; Cui, X.; Li, J.; Shi, X.; Qiao, Y. Method validation for the analysis of licorice acid in the blending process by near infrared diffuse reflectance spectroscopy. *Anal. Meth.* **2015**, *7*, 5830–5837. [[CrossRef](#)]
21. Luo, Y.; Li, W.; Huang, W.; Liu, X.; Song, Y.; Qu, H. Simultaneous assay of six components in water extract and alcohol precipitation liquid in *Astragali radix* by HPLC-UV-ELSD. *J. Chin. Mater. Med.* **2016**, *41*, 850–858.
22. Xu, Z.; Huang, W.; Gong, X.; Ye, T.; Qu, H.; Song, Y.; Liu, D.; Wang, G. Design space approach to optimize first ethanol precipitation process of Dangshen. *J. Chin. Mater. Med.* **2015**, *40*, 4411–4416.
23. Wang, K.Y.; Bian, X.H.; Tan, X.Y.; Wang, H.T.; Li, Y.K. A new ensemble modeling method for multivariate calibration of near infrared spectra. *Anal. Meth.* **2021**, *13*, 1374–1380. [[CrossRef](#)]
24. Gerretzen, J.; Szymanska, E.; Jansen, J.J.; Bart, J.; Manen, H.; Heuvel, E.R.; Buydens, L.M.C. Simple and Effective Way for Data Preprocessing Selection Based on Design of Experiments. *Anal. Chem. Acta* **2015**, *87*, 12096–12103. [[CrossRef](#)] [[PubMed](#)]
25. ISO 5725-1:1994; Accuracy (Trueness and Precision) of Measurement Methods and Results—Part 1: General Principles and Definitions. International Organization for Standardization: Geneva, Switzerland, 1994.
26. International Conference on Harmonisation (ICH) of Technical Requirements for Registration of Pharmaceuticals for Human Use, Topic Q2(R1): Validation of Analytical Methods: Text and Methodology; ICH: Geneva, Switzerland, 2005.
27. The European Agency for the Evaluation of Medicinal Products. *Note for Guideline on the Use of Near-Infrared Spectroscopy by the Pharmaceutical Industry and the Data Requirements for News Submissions and Variations*; European Agency for the Evaluation of Medicinal Products: London, UK, 2003.
28. Li, T.T.; Hu, T.; Nie, L.; Zang, L.X.; Zeng, Y.Z.; Zang, H.C. Rapid monitoring five components of ethanol precipitation process of Shenzhiling oral solution using near infrared spectroscopy. *Chin. J. Trad. Chin. Med.* **2016**, *41*, 3543–3550.
29. *Guide to the Expression of Uncertainty in Measurement*; ISO: Geneva, Switzerland, 1993.
30. Zhang, C.; Liu, F.; Qiu, Z.J.; He, Y. Application of Deep Learning in Food: A review. *Compr. Rev. Food Sci. Food Saf.* **2019**, *18*, 1793–1811.